

Object Tracking Using High Resolution Satellite Imagery

Lingfei Meng, *Student Member, IEEE*, and John P. Kerekes, *Senior Member, IEEE*

Abstract

High resolution multispectral satellite images with multi-angular look capability have tremendous potential applications. We present an object tracking algorithm that includes moving object estimation, target modeling, and target matching three-step processing. Potentially moving objects are first identified on the time-series images. The target is then modeled by extracting both spectral and spatial features. In the target matching procedure, the Bhattacharyya distance, histogram intersection, and pixel count similarity are combined in a novel regional operator design. Our algorithm has been tested using a set of multi-angular sequence images acquired by the WorldView-2 satellite. The tracking performance is analyzed by the calculation of recall, precision, and F_1 score of the test. In this study, we have demonstrated the capability of object tracking in a complex environment with the help of high resolution multispectral satellite imagery.

Index Terms

Object tracking, high resolution, multispectral satellite imagery

I. INTRODUCTION

Object tracking in a complex environment has long been an interesting and challenging problem [1]. In the remote sensing context, it has often been applied to the use of aerial or satellite imagery to track ground vehicle traffic [2]. Algorithms have been developed to demonstrate vehicle tracking using low-rate video or visible imagery sequences collected by sensors on aircraft [3]–[8]. Airborne spectral imagery [9], as well as spectral combined with polarimetric imaging [10], have also been used to demonstrate the capability of remote sensing platforms to track vehicles. In another application, satellite imagery [11] along with other data sources [12] have been used to track ships in the ocean. Additionally, synthetic aperture radar airborne and satellite sensors have also been shown to have surface object tracking capabilities [13].

Current satellite platforms offer limited utility for surface object tracking primarily due to inherent tradeoffs in resolution and spatial/temporal coverage. High resolution satellites located in low earth orbits with adequate resolution (~1 meter) to resolve surface objects offer limited spatial coverage (10's of sq. km.) and long repeat

intervals (days). Satellites with short repeat intervals (minutes) are located in geosynchronous orbits and offer poor ground resolution (~ 1 km). However, as satellite technology matures and more satellites are launched into orbit, it is appropriate to consider the possibilities for tracking surface objects offered by these new systems.

One example is the WorldView-2 (WV2) satellite which was launched by DigitalGlobe in 2009 [14]. WV2 collects one panchromatic and eight multispectral bands with center wavelengths at 425, 480, 545, 605, 660, 725, 835, and 950 nm. The collected panchromatic imagery has a spatial resolution of 0.5 m, and multispectral imagery has 2 m spatial resolution. WV2 overcomes some of the limitations for object tracking by satellite by providing the combination of high spatial and spectral resolution together with a very agile satellite platform. The agility of WV2 enables the capability of rapid retargeting which allows a sequence of images to be collected within minutes as the satellite passes over a given location [15]. All of these exciting features of WV2 provide a platform to further demonstrate the capability of object tracking with the help of spaceborne sensors.

In this work, we propose an object tracking algorithm for use with multitemporal and multispectral satellite imagery. Multiple objects can be tracked simultaneously with user-initialized starting points. At this point, the tracking algorithm only relies on the intensities of the pixels and does not include any kinematic capability to account for the smooth movement of the objects. The outline of the paper is as follows. In Section II, the proposed object tracking algorithm is introduced. Then in Section III the proposed algorithm is validated by performing object tracking on a set of WV2 multi-sequence images provided by DigitalGlobe. Discussion and conclusions are presented in Section IV.

II. OBJECT TRACKING PROBLEM FORMULATION

The proposed object tracking algorithm is illustrated in Fig. 1. The algorithm consists of three steps, which are moving object detection, target modeling, and target tracking. Potentially moving objects are first identified based on the time-series images. A reference target is then modeled by extracting spectral and spatial features. Finally a regional feature matching operator is applied to estimate the object motion trajectory. The algorithm is introduced below in detail.

A. Moving Object Detection

One of the approaches for detecting moving objects is to calculate the frame difference pixel by pixel. For a sequence of images $f(\mathbf{x}, t_1), \dots, f(\mathbf{x}, t_n)$ acquired from time t_1 to t_n , an accumulative difference image (ADI) can be formulated. The values of the ADI at location \mathbf{x} are counts, and can be calculated as [16]

$$A_j(\mathbf{x}) = \begin{cases} A_{j-1}(\mathbf{x}) + 1 & \text{if } [f(\mathbf{x}, t_r) - f(\mathbf{x}, t_j)] > \eta \\ A_{j-1}(\mathbf{x}) & \text{otherwise} \end{cases}, \quad (1)$$

where $A_j(\mathbf{x})$ is the ADI after the j th image $f(\mathbf{x}, t_j)$ in the sequence, $f(\mathbf{x}, t_r)$ is the reference image on which we want to find the moving objects, and η is the threshold, which is approximated to be 5% - 10% of the maximum image difference between the reference and the j th images in this work. For a sequence of images collected within

a short time frame, the ADI can be calculated based on the accumulation of all the frames. Any pixel with large ADI value is highly likely to be a moving object in the reference image. A threshold that is a count lower than the total number of frames can be further applied to the ADI to filter out the possible background pixels, and a binary mask image $M_i(\mathbf{x})$ can be found accordingly to highlight the moving objects. The filtered i th image in the sequence can be found as

$$f'(\mathbf{x}, t_i) = f(\mathbf{x}, t_i) \cdot M_i(\mathbf{x}). \quad (2)$$

In this work the moving object detection is performed on all the frames by iteratively using each frame as the reference image.

B. Target Model

The target is defined as the interested object to be tracked. The reference target can be represented by a user-defined region \mathbb{R} (window) centered at \mathbf{x}^* in the filtered first frame $f'(\mathbf{x}, t_1)$. The target model is represented by spectral and spatial features as illustrated in Fig. 1. The spectral and spatial features are defined below respectively.

The spectral feature is defined as the target's probability density function (PDF). The PDF of the reference target model is estimated by discrete densities, and m -bin histograms have been shown to be sufficient for object tracking purpose [17]. The m -bin histograms \mathbf{H}_b of the reference target model in the b th spectral band can be expressed as

$$\mathbf{H}_b = \{h_1, \dots, h_m\}_b \quad b = 1 \dots S, \quad (3)$$

where S is the number of spectral bands. The histogram of the l th bin in \mathbf{H}_b can be computed as

$$h_l = \sum_{i=1}^{N_t} K(|\mathbf{x}_i - \mathbf{x}^*|) \delta [\text{ind}(\mathbf{x}_i) - l], \quad (4)$$

where δ is the Kronecker delta function, $\text{ind}(\mathbf{x}_i)$ is the index of histogram bin associated with image intensity at location \mathbf{x}_i , $K(|\mathbf{x}_i - \mathbf{x}^*|)$ is the isotropic kernel which could be monotonic decreasing to reduce the background occlusion effect, or could be uniform to satisfy low computational cost, and N_t will be introduced in Eq. (5). In this paper a uniform kernel is used to accelerate the computation. The width of the kernel is determined by the size of the window. It should be noticed that only the target pixels are used for the calculation of h_l , and all the background pixels are eliminated.

The spatial feature is defined as the geometric area of the reference target surface in the window region \mathbb{R} , and is estimated based on its pixel count N_t which can be estimated as

$$N_t = \sum_{\mathbf{x} \in \mathbb{R}} \text{sgn} [f'(\mathbf{x}, t_1)], \quad (5)$$

where sgn is the signum function and is defined as

$$\text{sgn}(x) = \begin{cases} -1 & \text{if } x < 0 \\ 0 & \text{if } x = 0 \\ 1 & \text{if } x > 0 \end{cases} \quad (6)$$

Given the reference target model, we want to find a best matching target candidate window in other image sequences. The target candidate windows are those centered on potential moving objects identified in the ADI, and are also represented using both spectral and spatial features. The histogram of a target candidate centered at \mathbf{y} can be represented as

$$\mathbf{P}_b(\mathbf{y}) = \{p_1, \dots, p_m\}_b \quad b = 1 \dots S, \quad (7)$$

where p_l is the histogram of the l th bin in $\mathbf{P}_b(\mathbf{y})$. The pixel count of a target candidate centered at \mathbf{y} can also be estimated in a similar way as Eq. (5), and is denoted as $N(\mathbf{y})$.

C. Target Matching

A sliding window over other image sequences is used to indicate the possible presence of the reference target. A regional feature matching operator is applied to find the similarity between the target model and the pixels within the window. Three different metrics are used to define the operator. For spectral feature matching, Bhattacharyya distance and histogram intersection are used. The Bhattacharyya distance [17] can be found as

$$d_B(\mathbf{y}) = \frac{1}{S} \sum_{b=1}^S \sqrt{1 - \rho_B[\mathbf{H}_b, \mathbf{P}_b(\mathbf{y})]}, \quad (8)$$

where

$$\rho_B[\mathbf{H}_b, \mathbf{P}_b(\mathbf{y})] = \sum_{i=1}^m \sqrt{\frac{h_i \cdot p_i(\mathbf{y})}{\sum_{i=1}^m h_i \cdot \sum_{i=1}^m p_i(\mathbf{y})}}. \quad (9)$$

For Bhattacharyya distance, low values indicate good matching.

The histogram intersection [18] can be calculated using

$$d_I(\mathbf{y}) = \frac{1}{S} \sum_{b=1}^S \rho_I[\mathbf{H}_b, \mathbf{P}_b(\mathbf{y})], \quad (10)$$

where

$$\rho_I[\mathbf{H}_b, \mathbf{P}_b(\mathbf{y})] = \sum_{i=1}^m \min[h_i, p_i(\mathbf{y})]. \quad (11)$$

For histogram intersection, high values indicate good matching.

The spatial feature matching is based on the pixel count within the sliding window. As mentioned earlier, a pixel count of the reference target N_t and a pixel count of the moving object $N(\mathbf{y})$ can be estimated. It is assumed that

the potential target candidate and reference target should have similar pixel counts, even though the target has been moved or rotated. The similarity between the reference target and the potential region based on pixel count can be found as

$$d_P(\mathbf{y}) = 1 - \frac{|N(\mathbf{y}) - N_t|}{N_t}. \quad (12)$$

A threshold could be applied to $d_P(\mathbf{y})$ to filter out the pixels with low similarities. Regional maxima can then be found based on the $d_P(\mathbf{y})$ values. Regional maxima are defined as the connected pixels with a constant $d_P(\mathbf{y})$ value, and their boundary pixels all have lower $d_P(\mathbf{y})$ values [19]. A binary image $\text{RMAX}(\mathbf{y})$ can then be generated to identify the locations of regional maxima. For a small reference target which may occupy only a few pixels, it is quite possible that the edges of the background also will present high similarities in pixel count. An opening morphological filter is therefore optional to eliminate this edge effect in the $\text{RMAX}(\mathbf{y})$ binary image. The opening morphological filter is the erosion followed by the dilation. The definition of the erosion and dilation operators can be found in [16].

A regional matching operator is finally designed based on these three metrics, and can be defined as

$$\phi(\mathbf{y}) = \left\{ w_1 \cdot \left[1 - \hat{d}_B(\mathbf{y}) \right] + w_2 \cdot \hat{d}_I(\mathbf{y}) \right\} \cdot \text{RMAX}(\mathbf{y}), \quad (13)$$

where \hat{d}_B and \hat{d}_I are normalized Bhattacharyya distance and histogram intersection whose original values are divided by their maxima, and w_1 and w_2 are weighting coefficients. In this paper w_1 and w_2 are selected equally as 0.5. A high $\phi(\mathbf{y})$ value indicates a good matching with the target model.

III. RESULTS

To validate the object tracking algorithm, a set of WV2 images provided by DigitalGlobe as part of the IEEE DigitalGlobe 2011 Data Fusion Contest [20] has been used. The imagery was collected over Rio de Janeiro (Brazil) in January 2010. The image sequences were collected within a three minute time frame with satellite elevation angles of 44.7°, 56.0°, 81.4° in the forward direction, and 59.8° and 44.6° in the backward direction. The 16-bit multispectral 8-band images were used for object tracking. The images were geo-registered by DigitalGlobe but not corrected for parallax. Different subsets of images have been selected for our study. A subset collected over a harbor area as shown in Fig. 2 and a subset collected over an airport region as shown in Fig. 3 are used for algorithm validation.

To better explain the methodology introduced in the last section, some intermediate results of target matching in the second frame of the harbor region are presented in Fig. 4. In the RGB image as shown in Fig. 4 (a), the red outline indicate the interested ship target, whose target template is extracted based on the first frame. The binary mask image M_i , $1 - d_B$, d_I , RMAX after applying opening morphological filter, and the combined feature matching score ϕ , are also presented in Fig. 4. Note in Fig. 4 (b) there are many false detections due to uncorrected parallax effects. Because the ship within the red outline shows both high spectral and spatial similarities to the target template, it can be easily identified and tracked in Fig. 4 (f) based on its high feature matching score ϕ .

The ground truth of the interested moving targets has been identified manually per pixel in the image sequences. The performance of the proposed algorithm is analyzed on a per pixel basis by the recall and precision, which are calculated based on the number of true positives (tp), false positives (fp), and false negatives (fn). The recall (R) and precision (P) can be calculated as

$$R = \frac{tp}{tp + fn}, \quad (14)$$

$$P = \frac{tp}{tp + fp}. \quad (15)$$

A F_1 score [21] which is also called F -measure can then be found as

$$F_1 = 2 \cdot \frac{R \cdot P}{R + P}. \quad (16)$$

The harbor area was first selected for algorithm testing. The RGB image of the first frame is shown in Fig. 5 (a). Our task was to track the ship shown within the red outline. The actual size of the target and the size of the searching window are listed in Table. I. The target only occupies a few pixels, and exhibits very similar shape and intensity value with a large amount of other objects in the scene. Several other small objects have also been found to be moving in the following images. All these factors introduce significant difficulties for our tracking task. The estimated trajectory of the ship movement based on the proposed object tracking algorithm is shown in Fig. 5 (b). The calculated R , P , and F_1 values are evaluated based on 50 pixels that are identified as ship target in the last four frames, and are listed in Table II. It can be seen that the proposed algorithm has very high tracking accuracy.

We further analyze the algorithm in another subset of the images, which is the airport area. The RGB image of the first frame is shown in Fig. 6 (a). The aircraft within the white outline is denoted as aircraft A, and the other one within the red outline is denoted as aircraft B. The size of these two targets and the size of the searching window are listed in Table. I. These two aircraft were found to be moving simultaneously in this area, and could not be easily distinguished. Meanwhile, an amount of other aircraft with similar shape and spectral features were also present in the scene. We applied the proposed algorithm to the image sequences to track aircraft A and aircraft B simultaneously. The estimated movement trajectory of aircraft A is shown in Fig. 6 (b). Although some background pixels were mis-detected as moving objects due to parallax, aircraft A can be tracked very accurately. The estimated movement trajectory of aircraft B is shown in Fig. 6 (c). It can be seen that the aircraft B can also be tracked very well, except several false alarms are present in the image. It is noticed that aircraft A shows as a false alarm in the third frame, because it also presents a similar pose to the reference target model of aircraft B. The calculated R , P , and F_1 values are evaluated based on 324 pixels that are identified as aircraft A, and 265 pixels that are identified as aircraft B in the last four frames. They are listed in Table II. It can be seen that the overall tracking performance is satisfactory based on the relatively high F_1 scores.

TABLE I: Parameters of target template.

Target	Actual size (pixel)	Window (pixel \times pixel)
Ship	17	11 \times 11
Aircraft A	136	19 \times 19
Aircraft B	104	19 \times 19

TABLE II: Overall performance of the proposed algorithm.

Region	Object	R	P	F_1
Harbor	Ship	0.690	0.919	0.782
Airport	Aircraft A	0.833	0.495	0.621
	Aircraft B	0.925	0.435	0.592

IV. DISCUSSION AND CONCLUSIONS

We have presented an object tracking algorithm applied to a sequence of multispectral satellite images. This unique algorithm is developed for an optical multi-angular data set, and is designed based on moving object estimation, target modeling, and target matching three-step processing. Potentially moving objects are first identified on the time-series images. A reference target is then modeled by extracting spectral and spatial features. In the target matching procedure, the Bhattacharyya distance, histogram intersection, and pixel count similarity are combined in a novel regional operator design. The use of both spectral and spatial feature ensures better tracking accuracy than using each of them alone as has been observed in the intermediate results of target matching. Our algorithm has been tested using a set of multi-angular sequence images acquired by the WV2 satellite. Three different objects have been successfully tracked at two regions. The tracking performance is analyzed by the calculation of recall, precision, and F_1 score of the test.

While we acknowledge the results shown are for a single data set with a limited number of objects the preliminary results have demonstrated the capability of tracking objects in a complex environment with the help of high resolution multispectral satellite imagery. The technique introduced in this paper also has potential applications in other research areas, such as object velocity estimation, and traffic control. Based on the spatial resolution of the available data set and also the relatively long time interval between two frames, it is very difficult to visually identify identical objects with small geometric size in the image sequences. Tracking small objects, such as vehicles, in a more dense scene is more challenging, and will be considered in our future work, as will extensions of the algorithm to include a kinematic model to account for the smooth movement of objects.

REFERENCES

- [1] A. Yilmaz, O. Javed, and M. Shah, "Object tracking: A survey," *ACM Comput. Surv.*, vol. 38, Dec. 2006.
- [2] S. Hinz, R. Bamler, and U. Stilla, "Theme issue: Airborne and spaceborne traffic monitoring," *ISPRS Journal of Photogrammetry and Remote Sensing*, vol. 61, no. 3–4, pp. 135–280, 2006.
- [3] I. Szotka and M. Butenuth, "Tracking multiple vehicles in airborne image sequences of complex urban environments," in *2011 Joint Urban Remote Sensing Event (JURSE)*, Apr. 2011, pp. 13–16.
- [4] K. Palaniappan, F. Bunyak, P. Kumar, I. Ersoy, S. Jaeger, K. Ganguli, A. Haridas, J. Fraser, R. Rao, and G. Seetharaman, "Efficient feature extraction and likelihood fusion for vehicle tracking in low frame rate airborne video," in *13th Conference on Information Fusion (FUSION)*, Jul. 2010, pp. 1–8.
- [5] K. Palaniappan, R. Rao, and G. Seetharaman, "Wide-Area Persistent Airborne Video: Architecture and Challenges," in *Distributed Video Sensor Networks*, B. Bhanu et al, Ed. Springer London, 2011, pp. 349–371.
- [6] C. Carrano, "Ultra-scale vehicle tracking in low spatial resolution and low frame-rate overhead video," in *Proc. SPIE*, vol. 7445, 744504, 2009.
- [7] J. Xiao, H. Cheng, H. Sawhney, and F. Han, "Vehicle detection and tracking in wide field-of-view aerial video," in *2010 IEEE Conference on Computer Vision and Pattern Recognition (CVPR)*, Jun. 2010, pp. 679–684.
- [8] D. Lenhart, S. Hinz, J. Leitloff, and U. Stilla, "Automatic traffic monitoring based on aerial image sequences," *Pattern Recognition and Image Analysis*, vol. 18, pp. 400–405, 2008.
- [9] J. Kerekes, M. Muldowney, K. Strackerhan, L. Smith, and B. Leahy, "Vehicle tracking with multi-temporal hyperspectral imagery," in *Proc. SPIE*, vol. 6233, 62330C, 2006.
- [10] M. Presnar, A. Raisanen, D. Pogorzala, J. Kerekes, and A. Rice, "Dynamic scene generation, multimodal sensor design, and target tracking demonstration for hyperspectral/polarimetric performance-driven sensing" in *Proc. SPIE*, vol. 7672, 76720T, 2010.
- [11] A. Liu, C. Peng, and S. Chang, "Wavelet analysis of satellite images for coastal watch," *IEEE Journal of Oceanic Engineering*, vol. 22, no. 1, pp. 9–17, Jan. 1997.
- [12] M. Bruno, K. W. Chung, H. Salloum, A. Sedunov, N. Sedunov, A. Sutin, H. Graber, and P. Mallas, "Concurrent use of satellite imaging and passive acoustics for maritime domain awareness," in *2010 International Waterside Security Conference (WSS)*, Nov. 2010, pp. 1–8.
- [13] S. Hinz, D. Weihing, S. Suchandt, and R. Bamler, "Detection and velocity estimation of moving vehicles in high-resolution spaceborne synthetic aperture radar data," in *2008 Computer Vision and Pattern Recognition Workshops*, Jun. 2008, pp. 1–6.
- [14] G. Marchisio, F. Pacifici, and C. Padwick, "On the relative predictive value of the new spectral bands in the worldview-2 sensor," in *2010 IEEE International Geoscience and Remote Sensing Symposium*, Jul. 2010, pp. 2723–2726.
- [15] N. Longbotham, C. Bleiler, C. Chaapel, C. Padwick, W. Emery, and F. Pacifici, "Spatial classification of worldview-2 multi-angle sequence," in *2011 Joint Urban Remote Sensing Event (JURSE)*, Apr. 2011, pp. 105–108.
- [16] R. C. Gonzalez and R. E. Woods, *Digital Image Processing*, 3rd ed. Upper Saddle River, NJ, USA: Prentice-Hall, Inc., 2006.
- [17] D. Comaniciu, V. Ramesh, and P. Meer, "Kernel-based object tracking," *IEEE Trans. Pattern Anal. Mach. Intell.*, vol. 25, no. 5, pp. 564–577, May 2003.
- [18] B. Schiele and J. L. Crowley, "Object recognition using multidimensional receptive field histograms," in *European Conference on Computer Vision*, 1996, pp. 610–619.
- [19] P. Soille, *Morphological Image Analysis: Principles and Applications*, 2nd ed. Secaucus, NJ, USA: Springer-Verlag New York, Inc., 2003.
- [20] <http://www.grss-ieee.org/2011-ieee-digitalglobe-data-fusion-contest/>
- [21] C. J. Van. Rijsbergen, *Information Retrieval*, 2nd ed. Newton, MA, USA: Butterworth-Heinemann, 1979.

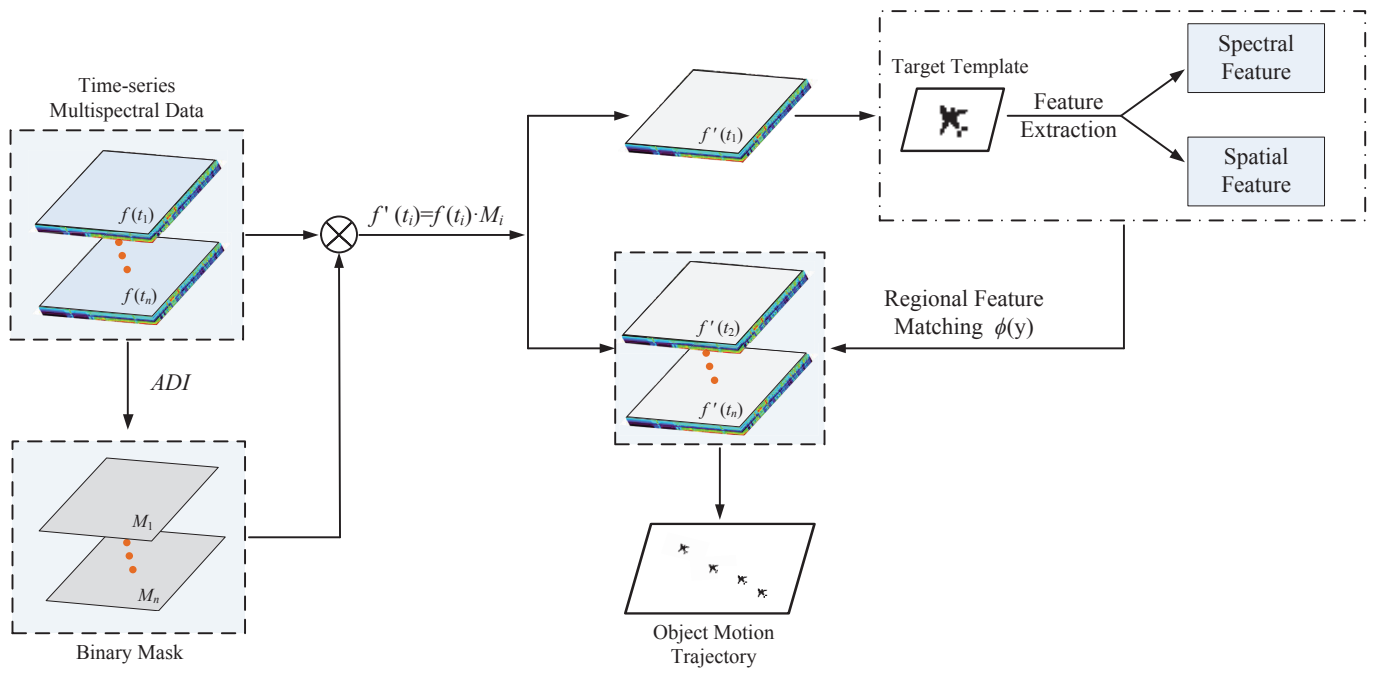


Fig. 1: Flowchart of the proposed object tracking algorithm.

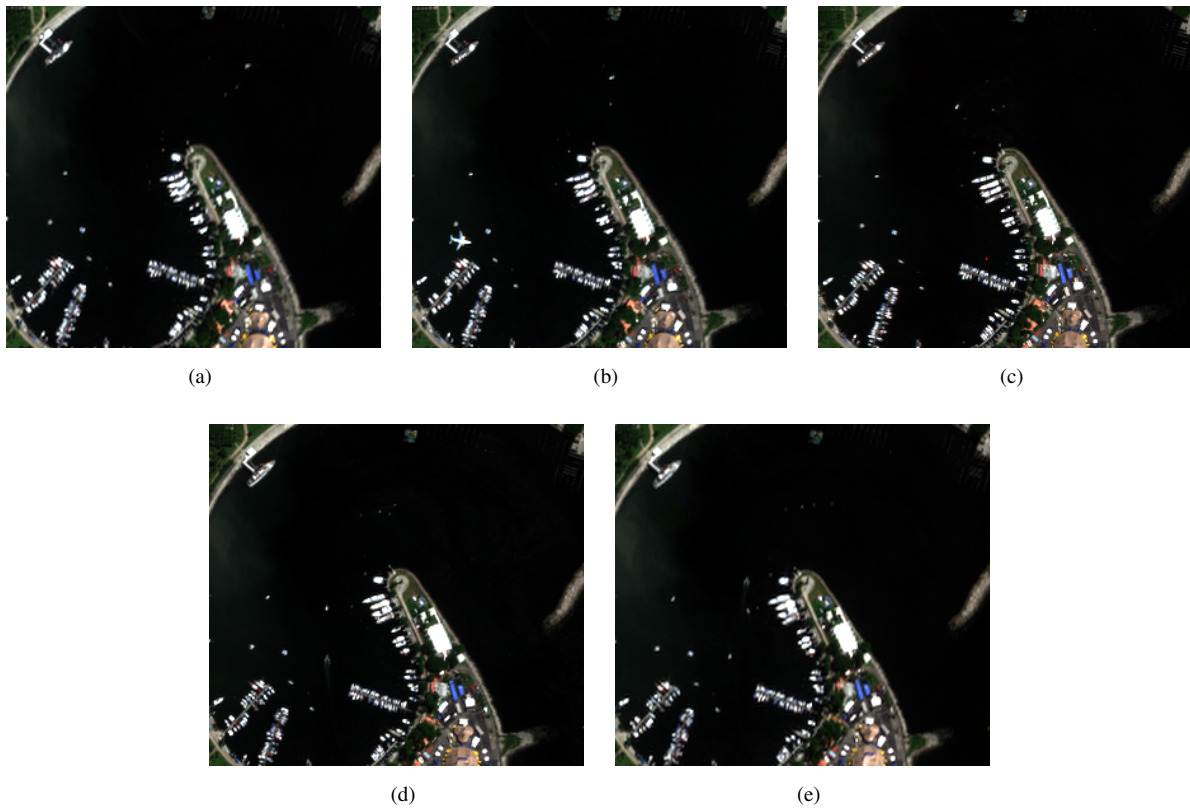


Fig. 2: Subsets of five frames collected over a harbor region at different times (a) 13:09:23, (b) 13:09:54, (c) 13:10:46, (d) 13:12:00, and (e) 13:12:41. All times are local.

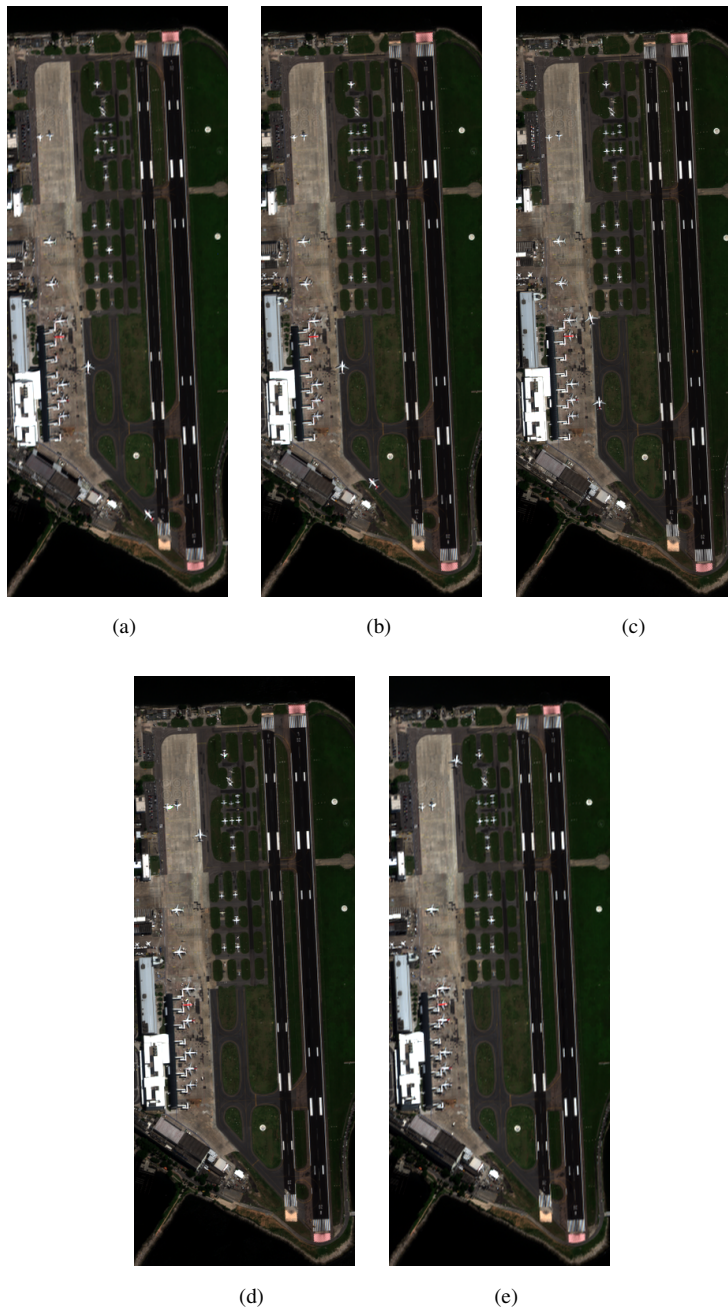


Fig. 3: Subset of five frames collected over an airport region at different times (a) 13:09:23, (b) 13:09:54, (c) 13:10:46, (d) 13:12:00, and (e) 13:12:41. All times are local.

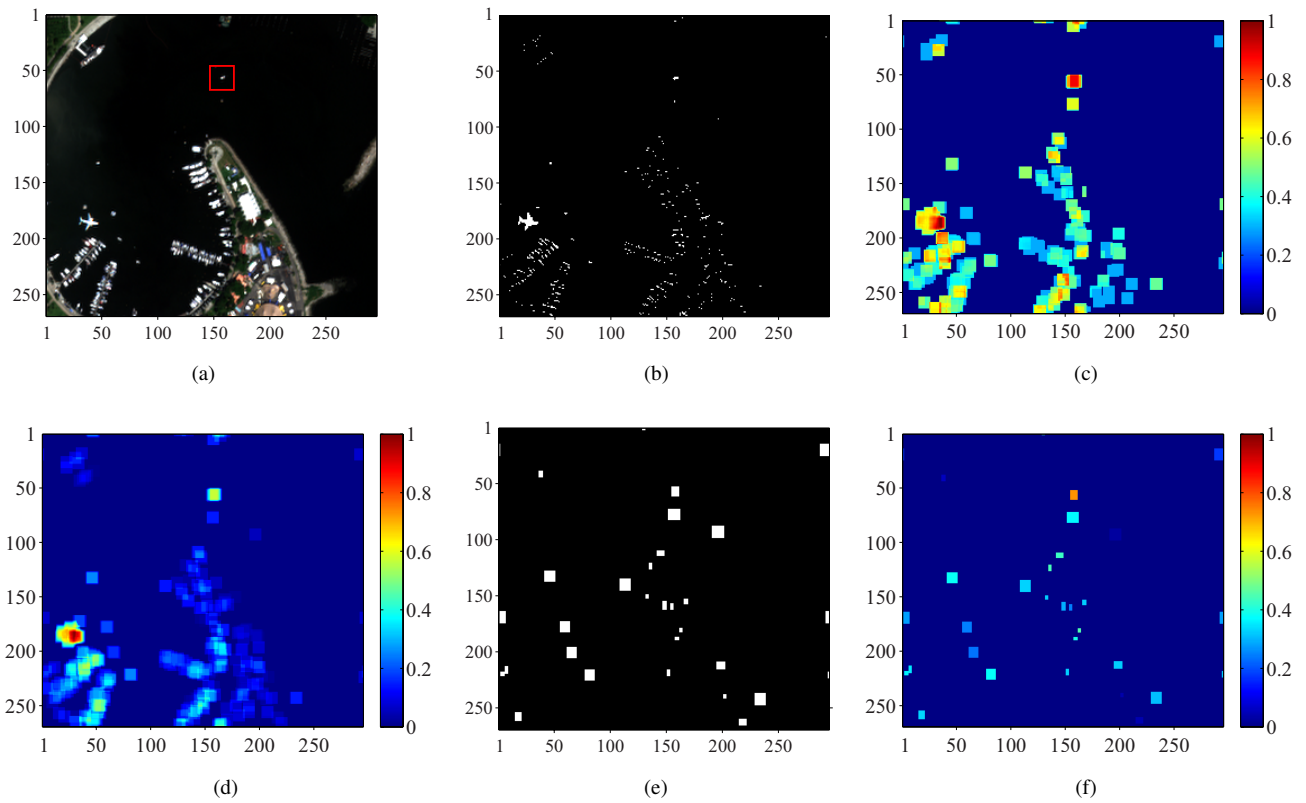
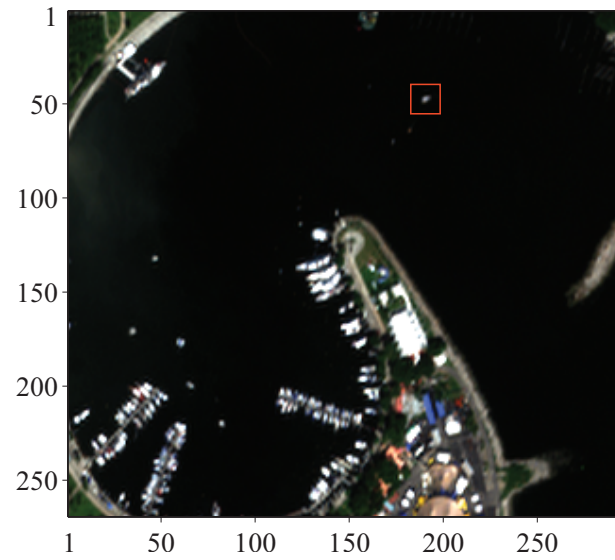
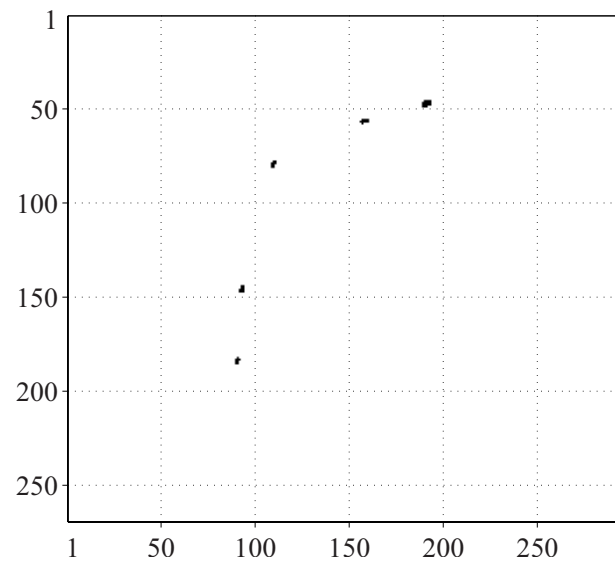


Fig. 4: Intermediate results of target matching in the second frame of harbor region. The target template is extracted based on the first frame. (a) RGB image. The red outline indicates the interested ship target. (b) Binary mask image M_i . (c) $1 - d_B$. (d) d_I . (e) RMAX. (f) Combined feature matching score ϕ .



(a)



(b)

Fig. 5: Ship tracking in the harbor area. (a) Harbor area RGB image, where the ship is within red outline. (b) Ship movement trajectory.

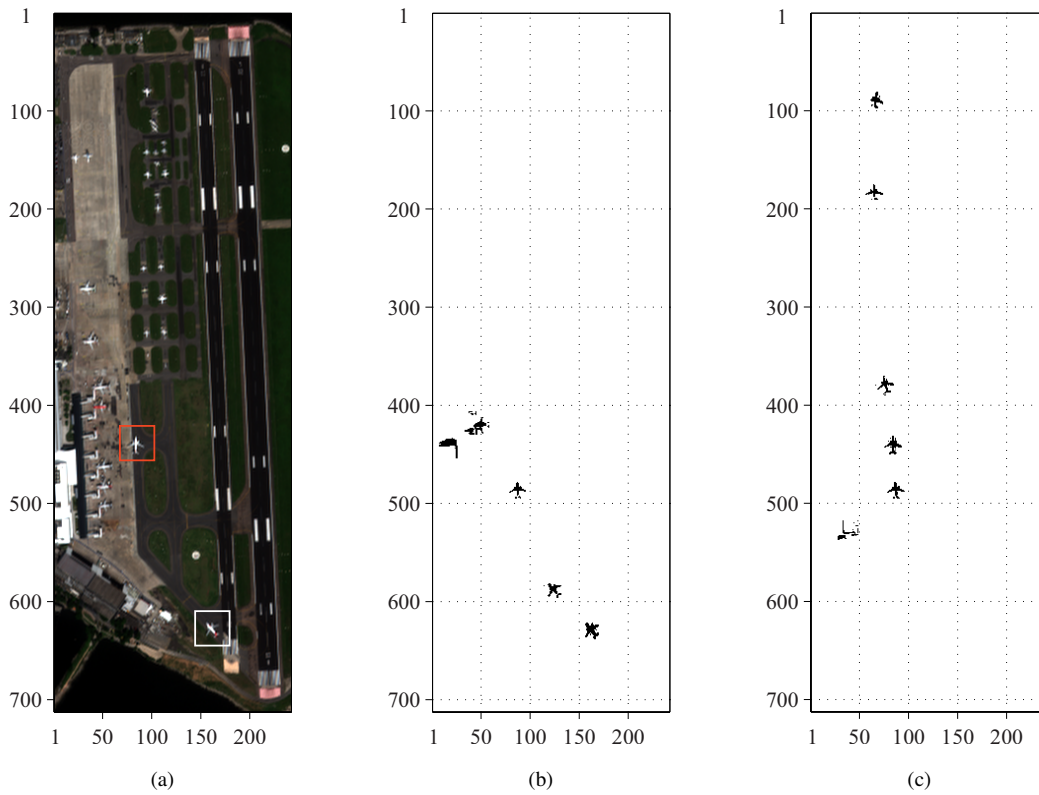


Fig. 6: Aircraft tracking in the airport area. (a) Airport area RGB image, where aircraft A is within the white outline and aircraft B is within the red outline. (b) Aircraft A movement trajectory. (c) Aircraft B movement trajectory.



Lingfei Meng (S'10) received the B.S. degree in electrical engineering from the Tianjin University, Tianjin, China, in 2007. He is currently working toward the Ph.D. degree in imaging science at the Rochester Institute of Technology, Rochester, NY.

From June 2011 to August 2011, he was a Research Intern with Ricoh Innovations, Inc., Menlo Park, CA. His research interests include imaging system modeling, digital image processing, and computer vision.

Mr. Meng was one of the winners of the 2011 IEEE GEOSCIENCE AND REMOTE SENSING Data Fusion Contest. He has served as a Reviewer for the IEEE TRANSACTIONS ON GEOSCIENCE AND REMOTE SENSING, IEEE JOURNAL OF SELECTED TOPICS IN APPLIED EARTH OBSERVATIONS AND REMOTE SENSING, AND JOURNAL OF THE OPTICAL SOCIETY OF AMERICA

A.



John P. Kerekes (S'81-M'89-SM'00) received the B.S., M.S., and Ph.D. degrees in electrical engineering from Purdue University, West Lafayette, IN, in 1983, 1986, and 1989.

From 1983 to 1984, he was a Member of the Technical Staff with the Space and Communications Group, Hughes Aircraft Co., El Segundo, CA, where he performed circuit design for communications satellites. From 1986 to 1989, he was a Graduate Research Assistant, working with both the School of Electrical Engineering and the Laboratory for Applications of Remote Sensing at Purdue University. From 1989 to 2004, he was a Technical Staff Member with the Lincoln Laboratory, Massachusetts Institute of Technology, Lexington, MA. In 2004, he became an Associate

Professor in the Chester F. Carlson Center for Imaging Science, Rochester Institute of Technology, Rochester, NY. His research interests include the modeling and analysis of remote sensing system performance in pattern recognition and geophysical parameter retrieval applications.

Dr. Kerekes is a member of Tau Beta Phi, Eta Kappa Nu, the American Geophysical Union, and the American Society for Photogrammetry and Remote Sensing. He is a Senior Member of the Optical Society of America and SPIE. From 1995 to 2004, he served as the Chair of the Boston Section Chapter of the IEEE Geoscience and Remote Sensing Society (GRSS), and from 2007 to 2010 he served as the founding Chair of the Western New York Chapter of GRSS. He was a Co-General Chair of IGARSS 2008 held in Boston, MA. He is currently a member of the GRSS Administrative Committee (AdCom) and is serving as the Vice President of Technical Activities of the GRSS.